Design and implementation of bound-to-quasibound GaN/AlGaN photovoltaic quantum well infrared photodetectors operating in the short wavelength infrared range at room temperature

Piotr Mensz, Ben Dror, Akhil Ajay, Catherine Bougerol, Eva Monroy, Meir Orenstein, Gad Bahir

Journal of Applied Physics ARTICLE scitation.org/journal/jap

Design and implementation of bound-to-quasibound GaN/AlGaN photovoltaic quantum well infrared photodetectors operating in the short wavelength infrared range at room temperature

Cite as: J. Appl. Phys. **125**, 174505 (2019); doi: 10.1063/1.5079408
Submitted: 30 October 2018 · Accepted: 11 April 2019 ·
Published Online: 6 May 2019

Piotr M. Mensz,[1,a)] Ben Dror,[1] Akhil Ajay,[2] Catherine Bougerol,[3] Eva Monroy,[2] Meir Orenstein,[1] and Gad Bahir[1]

AFFILIATIONS

[1]Department of Electrical Engineering, Technion-Israel Institute of Technology, Haifa 32000, Israel
[2]Univ. Grenoble-Alpes, CEA, INAC, PHELIQS, 17 av. des Martyrs, 38000 Grenoble, France
[3]Univ. Grenoble-Alpes, CNRS-Institut Néel, 25 av. des Martyrs, 38000 Grenoble, France

[a)]**Author to whom correspondence should be addressed:** pmensz@gmail.com

ABSTRACT

In this paper, we discuss the design of photovoltaic quantum well infrared photodetectors (QWIPs) based on polar GaN/AlGaN multiquantum wells (MQWs). Getting a reasonable escape probability of the excited electron requires adjusting the bound-to-quasibound intersubband transition in the absorbing quantum well and engineering the polarization-related internal electric field in the barriers. This can be achieved with a MQW period that consists of 3 layers, namely, the active quantum well, an extraction barrier, and an injection barrier, the latter being thin enough to allow tunneling transport. Following this design scheme, we demonstrate bound-to-quasibound GaN/AlGaN QWIPs with peak photocurrent response at 2.3 μm, operating at room temperature in both photovoltaic and photoconductive modes. Based on high-resolution x-ray diffraction measurements, the entire detector structure, which included a 40-period MQW with 30 nm-thick barriers, along with top and bottom contact layers of combined thickness above 900 nm, was grown pseudomorphically on an AlGaN-on-sapphire template. A room-temperature responsivity of 88 μA/W was measured at zero bias, increasing up to 302 μA/W at −1.0 V bias. The responsivity reached its maximum at 150–200 K, where it was approximately a factor of 2 higher than at room temperature. Ideas for a new device structure to improve the QWIP response in the photovoltaic mode are proposed.

I. INTRODUCTION

The expansion of the field of III-nitride optoelectronics started in the mid-1990s with the demonstration and commercialization of blue light emitting diodes (LEDs) and laser diodes (LDs), full-color LED displays, and white-light LEDs for lighting.[1] The interest of III-nitride semiconductors for optoelectronic devices stems from their direct, wide bandgap energy, which can be tuned from 0.7 eV for InN up to 6.2 eV for AlN. III-nitride devices, particularly LEDs and LDs, demonstrated high emission efficiency, performance stability, robustness at outdoor environment, long lifetime, and low production cost. In addition to their success in the domain of optoelectronics, III-nitrides also became a main candidate for the next generation of high speed, power electronics, and wireless communication devices in the THz band.[1,2] GaN/AlGaN heterostructure field effect transistors (HFETs) provide the highest value of frequency × power product among commonly used semiconductors, combined with high electron saturation velocity, breakdown voltage, and operation temperature.[3] An important advantage of the GaN/AlGaN technology is the possibility of growing of heterostructure devices epitaxially on large Si substrates,[4,5] which increases interest not only for microelectronics, but also in the field of photonic devices on silicon, in particular, visible/ultraviolet emitters and solar-blind ultraviolet photodetectors, including focal-plane arrays (FPAs) for camera chips.[6]

Infrared (IR) photodetection in III-nitrides usually takes advantage of intersubband transitions (ISBTs) in GaN/AlGaN multiquantum wells (MQWs). For this application, the GaN/AlN system offers room-temperature operation, thanks to the nearly 2 eV conduction band offset and large longitudinal-optical (LO) phonon energy (92 meV in GaN).[3] Furthermore, the intersubband relaxation time in GaN/AlGaN QWs can be very short, below 150 fs,[7] which is an order of magnitude shorter than the transient times obtained for InGaAs QWs.[7]

The concept of quantum well infrared photodetectors (QWIPs) based on ISBTs was proven using GaAs/AlGaAs.[8] Photoconductive GaAs/AlGaAs QWIP FPAs have found their niche application in Medium Wavelength Infrared and Long Wavelength Infrared thermal imaging, used in certain military and aerospace applications.[9,10] However, there are difficulties in introducing QWIP FPAs in the market, since the detection efficiency of QWIPs is lower than that of interband photodetectors and their high dark current tends to saturate the capacitors in read-out integrated circuits (ROIC).[6]

In principle, the problem of ROIC saturation can be lifted, if the detector has good performance in photovoltaic (PV) mode, but obtaining high responsivity and detectivity in a PV QWIP is a challenge. PV detection in QWIPs was studied in asymmetric GaAs/AlGaAs MQW structures, typically by the addition of an extra barrier or two, often combined with extra doping in the outer barrier (modulation doping). As a result of the Coulomb attraction between free carriers in the quantum well (QW) and ionized donors in the outer barrier, an electric field develops across the outer barriers of the detector, which favors the drift of the photoexcited electrons at zero bias.[11,12] Thus, using asymmetric-barrier GaAs/AlGaAs PV-QWIPs, under 45° front illumination at $\lambda_{peak} = 10\,\mu$m, 50 mA/W responsivity, and 2.5×10^9 Jones (cm $Hz^{1/2}$ W^{-1}) detectivity were demonstrated at 77 K.[12] Using modulation-doped double-heterostructure PV-QWIP implemented in GaAs/AlAs/AlGaAs, Luna *et al.*[13] demonstrated 50 mA/W responsivity and 2.0×10^{12} Jones detectivity, under 45° front illumination at $\lambda_{peak} = 4.5\,\mu$m, at 25 K.[13] Later, Lai *et al.*[14] reported strong PV response from double-heterostructure PV-QWIPs implemented in a strain-compensated AlAs/$In_{0.84}Ga_{0.16}As$/AlAs/$In_{0.52}Al0_{.48}As$ MQW structure, with peak detection at 2.09 μm. Their responsivity was 250 mA/W, with a detectivity of 3.0×10^{12} Jones at 77 K and 7.0×10^9 Jones at 270 K, respectively. The incident light was coupled to the QWIP active region through a 45° lapped edge facet.[14]

In the case of III-nitrides, photoconductive ISB detectors were first demonstrated in a wurtzite GaN/AlGaN (2 nm/2 nm) short-period MQW structure with light detection in the short wavelength infrared (SWIR)[15] range (peak wavelength 1.90 μm). Detection relied on absorption between the ground and first-excited states localized in the GaN wells, and the weak tunneling probability between QW excited states. Unfortunately, the high leakage current, associated with the high dislocation density, made the result difficult to reproduce. GaN/AlGaN classical photoconductive QWIPs, based on the escape of excited-state electrons from the QW to the conduction band of the AlGaN barrier have been demonstrated in the THz range (at wavelengths $\lambda > 20\,\mu$m)[17] using the 20 repetition MQW structure with 5 MLs of GaN and 22 MLs of $Al_{0.08}Ga_{0.92}N$ "step-well," and 5 MLs of $Al_{0.16}Ga_{0.84}N$ and 38 MLs of $Al_{0.08}Ga_{0.92}N$ "step barrier," constituting approximately 18 nm-thick period MQW, grown on bulk GaN substrates. In the case of QWIP operating in the THz spectral range, the lattice mismatch of the required $Al_xGa_{1-x}N$ material is significantly smaller than in the case of QWIP-on-AlN substrate, operating in SWIR, and it is, therefore, possible to fabricate the MQW QWIP device structure with low defect density in the GaN-active regions.

In the SWIR, GaN/AlN PV-QWIPs operating at room temperature at peak wavelength around 1.9 μm have been demonstrated.[16] The operation of these detectors relies on the asymmetry of the potential in polar GaN QWs, due to the spontaneous and piezoelectric polarization. The excitation of an electron into the upper quantized level is accompanied by the weak effect of a microscopic charge displacement in the growth direction, which for high electron density in QW and a large number of QWs, can be detected as an external photovoltage. Thus, the PV effect in this detector does not rely on the escape probability of the excited electrons.[16] An alternative PV photodetector is the quantum cascade detector (QCD), based on ISB absorption and "cascading" between separate QWs subbands, mediated by phonon emission.[18] SWIR GaN/AlGaN QCDs have been reported.[19,20] A QCD based on ISB electron scattering in a 15 nm-wide AlN/AlGaN/AlN single polarized QW extractor was also implemented.[21] These devices take advantage of the polarization-induced internal electric field to design an efficient AlGaN electron extractor, where the energy levels are separated by more than the LO-phonon energy.

Most experimental results of ISBT in GaN/AlGaN MQWs were obtained from the epitaxial wurtzite structures grown on hexagonal c-plane substrates.[22] Such MQWs exhibit high internal electric field due to the high spontaneous polarization and piezoelectric constants in these materials. There are also reports on intersubband absorption or photocurrent measurements in semipolar[23,24] or nonpolar[25–29] GaN/AlGaN MQWs. Theoretical calculations for ISBT in nonpolar QWs usually show higher values for the optical matrix element compared to polar QWs. However, the improvement has not been clearly demonstrated in absorption or photocurrent measurements, likely because of structural defects and strong alloy inhomogeneity induced by the larger lattice mismatch in the nonpolar orientations with respect to the polar axis. Last but not least, polar AlGaN/GaN structures can be grown on Si(111) substrates,[4,5] which opens the opportunity of integration with mature silicon technology. Thus, it seems worthwhile to deal with polar GaN/AlGaN heterostructures via band, strain, and polarization engineering, rather than trying to escape from it.

In this paper, we discuss the design of GaN/AlGaN PV-QWIPs grown along the polar crystallographic axis, trying to engineer the bands to improve the probability of escape of the excited electron, while keeping the structure asymmetric enough to obtain a reasonable photocurrent at zero bias. The experimental realization of the devices is presented and potential improvements are discussed.

II. DESIGN OF PHOTOVOLTAIC QWIP

For the design of efficient QWIP detector, we must keep in mind that a high probability of photon absorption in the active QW requires "bound-to-bound" ISBTs. On the other hand, high escape probability from the excited state of the absorbing well to the

conduction band of the barrier requires the wavefunction of the excited state to be extended into the barrier conduction band.[8] Therefore, efficient QWIP design requires a compromise with respect to the excited-state localization. In order to quantify this procedure, we need to maximize the product of both probabilities: "absorption" and "escape." This resulted in a concept called "bound-to-quasibound" ISBT[8] in III–V QWIP devices, which among other advantages is supposed to give an optimal signal-to-noise ratio.[8,30] In this concept, the wavefunction of the excited state still has a high amplitude in the absorbing well, but it has a tail that extends into the conduction band of the barrier.

Our design is based on a self-consistent solution of the 1-dimensional 8×8 k·p Schrödinger-Poison equations using the envelope function approximation for strained polar GaN/AlGaN MQWs. We used a commercial solver,[31] which applies a standard finite difference method to discretize the coupled partial differential equations and solve them, using the Newton-Raphson algorithm. Typically, five to seven periods of MQW were included in the calculations, with periodic boundary conditions. The material parameters used in the input are those reported by Kandaswamy *et al.*[32]

Consider the conduction band profile of a polar GaN/$Al_{0.4}Ga_{0.6}N$ (1.56 nm/30 nm) MQW, which is presented in Fig. 1(a). It exhibits a saw-tooth potential profile due to the strong internal electric field, with opposite sign in the GaN wells and in the $Al_{0.4}Ga_{0.6}N$ barriers. Only the ground state is strongly localized in the GaN wells, but the potential profile does not favor the generation of photocurrent after ISB absorption. In the barrier, there are many excited states, but electron escape is only possible for the topmost energy states in the figure, and the optical transition matrix element for ISBT from the ground state to these high-energy final states is very low.

In view of this band structure, it is clear that designing QWIP using polar GaN/AlGaN MQWs requires either compensating the internal electric field along the c-direction, or some band engineering to use it to the device advantage. Besides, the GaN/AlN system is strongly lattice mismatched (about 2.6% in-plane mismatch), which imposes certain limitations in the layer thickness and composition in order to reduce structural defects associated with strain relaxation.

Starting from the basic structure in Fig. 1(a), if we insert an $Al_{0.71}Ga_{0.29}N$ layer with a thickness of 5 monolayers (ML, 1 ML $\approx$ 0.25 nm) between the GaN well and the $Al_{0.4}Ga_{0.6}N$ barrier, as shown Fig. 1(b), the potential profile shows a distinct reduction in internal electric field in the $Al_{0.4}Ga_{0.6}N$ barrier. In fact, by proper design, the field can be reduced to zero.[33] Let us call this inserted $Al_{0.71}Ga_{0.29}N$ layer an "injection barrier," while the $Al_{0.4}Ga_{0.6}N$ layer will be the "escape barrier." By adjusting the thickness and composition of the injection barrier, it is possible to control the electric field in the $Al_{0.4}Ga_{0.6}N$ escape barrier.[17,22] In our case, we set a moderate internal field of 25 kV/cm in the escape barrier, in order to observe a photovoltaic effect by favoring the escape of the excited electron even without external bias. At the end of this passage, this photoelectron can tunnel through the potential formed by the injection barrier, to enter the next MQW period, where it can recombine in the well or escape again.

From the eigen-energy values calculated by the simulation, as shown in Fig. 1(b), we expect the photo-absorption peak energy to be at $E_{ph} = E_2 - E_1 \approx 0.54$ eV, corresponding to the energy separation of two lowest eigenstates in the absorbing well. This transition was set to be a bound-to-quasibound ISBT, as the ground state is strongly localized, while the excited state extends into the barriers.

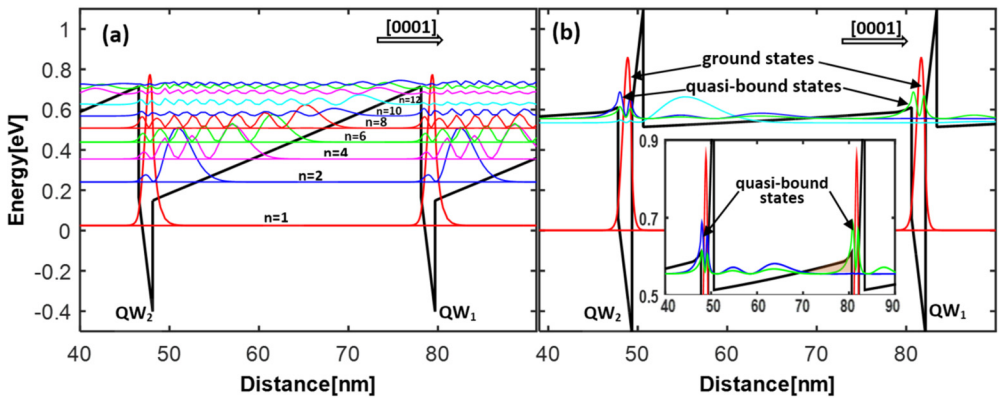

FIG. 1. (a) Conduction band diagram (black, thick line) of polar GaN/$Al_{0.4}Ga_{0.6}N$ MQWs grown on an $Al_{0.4}Ga_{0.6}N$ template on the [1000] sapphire plane. The black block arrow indicates the growth direction. Selected squared wavefunctions of the stationary quantum states formed in the wide triangular potential well are plotted with various color lines. They are obtained from self-consistent solving of 1D Schrödinger and Poison equations. These squared wavefunctions relate to envelope functions of two-dimensional subbands confined in a wide triangular potential formed in polarized AlGaN barrier of the MQW structure, instead of GaN well. The sequence of the quantum numbers for various subbands localized in this region is specified from $n = 1$, for the ground state, up to $n = 12$, for the nearly extended state. There is no quasibound states, for this potential and optical matrix elements for transition from the ground state to the lowest extended states are very small. (b) By insertion of a 5-ML-thick $Al_{.71}Ga_{.29}N$ tunneling barrier between well and barrier layers, the strong polarization in $Al_{0.4}Ga_{0.6}N$ barrier can be virtually eliminated or adjusted to the desirable internal field to obtain QWIP operation in PV mode. The quasibound states (green and blue lines) are indicated in the conduction band of this structure. Inset: Enhanced view of the conduction band edge with the squared wavefunction of the quasibound excited states. They are partly localized in the GaN-QW, while their tails extend through entire AlGaN barrier conduction band. The triangular-shape tunneling barrier for the excited-state electrons in order to escape from the well is highlighted in light brown.

In the well region, the quasibound state square wavefunction shows double-peak-shape, which is characteristic to the first-excited state in the QW, but its energy level, especially away from the well, resides above the barrier conduction band edge [see the inset of Fig 1(b)].

For the design, we assume direct n-doping of the GaN well at the donor concentration level $N_d = 5 \times 1018\ cm^{-3}$ and additional n-type modulation doping in the $Al_{0.4}Ga_{0.6}N$ escape barrier [at the level of $N_d = 5 \times 1018\ cm^{-3}$ over 1 nm space, set back from the well interface by 1 nm distance; see the layer diagram in Fig. 2(a)]. Modulation donor doping in the barrier facilitates additional electron accumulation in the well. Simultaneously, it originates a strong electric field (>10^5 V/cm) at the 1 nm-thick "set back" region of AlGaN-escape barrier near the well, because of Coulomb attraction between the electrons in the well and the parent ionized Si-donors in the barrier. This extra electric field adds to the spontaneous polarization and piezoelectric field already existing in the polar AlGaN-escape barrier [see the area highlighted in light brown in the inset in Fig 1(b)].

The proper device design requires probability for the photoexcited electron to tunnel through the triangular potential barrier [to the left in Fig.1(b)] with higher probability than to "tunnel back" across the $Al_{0.71}Ga_{0.29}N$ injection barrier [to the right in Fig 1(b)]. The photoexcited electrons, which managed to overcome the triangular potential barrier, continue their drift toward the next QW, thanks to the internal polarization field existing in the center of $Al_{0.4}Ga_{0.6}N$ escape barrier. Thus, without applying voltage bias, a net electronic current can develop in the $Al_{0.4}Ga_{0.6}N$ escape barrier (which is the bases of the proposed photovoltaic QWIP).

Figure 2(a) summarizes the epitaxial layer design of the GaN/AlGaN QWIP. The bottom contacting layer was 690-nm-thick n^+-$Al_{0.4}Ga_{0.6}N$, Si-doped at $1 \times 10^{19}\ cm^{-3}$. The MQW structure contains 40 periods of the 3-layer heterostructure (6-ML-thick GaN well, 30-nm-thick $Al_{0.4}Ga_{0.6}N$ escape barrier, and 5-ML-thick $Al_{0.71}Ga_{0.29}N$ injection barrier), followed by a 4-ML-thick n^+-GaN "injection well," Si-doped at $5 \times 10^{18}\ cm^{-3}$ and a 200-nm-thick "cap layer" of n^+-$Al_{0.4}Ga_{0.6}N$, doped at $1 \times 10^{19}\ cm^{-3}$.

Designing a device in the polar direction requires a consideration of the effect of polarization in all the layers, not only in the active MQW. In this case, since the QWIP is designed to operate at zero bias, any substantial potential barrier blocking electron injection or extraction would reduce the current flow across the entire device. In our design, there is no barrier for electrons extraction at the bottom n^+-contact layer, but the direct deposition of an $Al_{.40}Ga_{.60}N$ cap layer on the topmost $Al_{.71}Ga_{.29}N$ injection barrier would result in a potential barrier for electron injection, as illustrated by the dashed-line band diagram in Fig. 2(b). Such barriers can be eliminated by the insertion of a 4-ML-thick n^+-GaN "injection well" between the cap layer and the MQW. Moreover, the injection well is strongly coupled with the first absorbing well, as shown in Fig. 2(b). In practical terms, it means they share

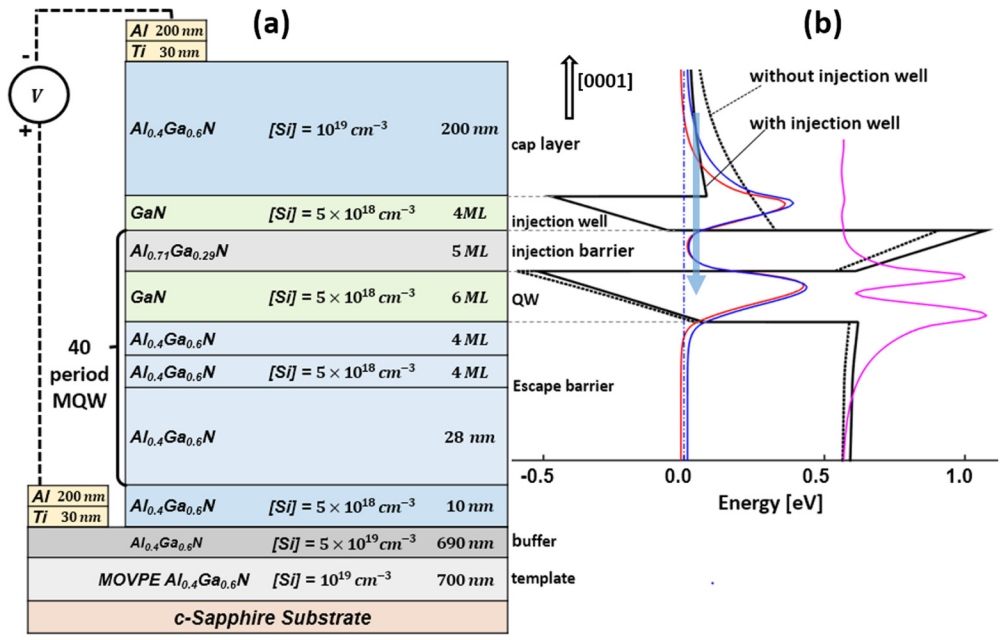

FIG. 2. (a) Schematic of the PV QWIP, grown along the [0001] axis, including the Ti/Al electrical contacts. The black block arrow indicates the growth direction. (b) Conduction band (CB) profile of the top contacting AlGaN/GaN layers with relevant squared wavefunctions (blue, red, and magenta lines). The dash-dotted line depicts the Fermi level position at zero voltage bias. A dotted line represents the band profile without the GaN "injection well." The "injection well" is essential to suppress the depletion region induced by the topmost $Al_{0.71}Ga_{0.29}N$ injection barrier in the cap layer, in order to improve the top contact resistance at zero bias. In addition, it facilitates the resonant tunneling contact electrons into the PV QWIP at zero bias by resonant tunneling. Namely, the injection and absorbing well shares their electrons because of the strong overlapping of their electronic wavefunctions (see the blue and red lines). The blue arrow indicates this electron injection from the top cap layer into the first absorbing well under illumination condition.

TABLE I. Specific layer parameters for the two QWIP designs: QWIP-on-AlGaN (top row) and QWIP-on-AlN (bottom row).

	Template	Buffer layer	Periods	Injection barrier	Active well	Escape barrier	Injection well	Cap layer
Composition	$Al_{0.4}Ga_{0.6}N$	$Al_{0.4}Ga_{0.6}N$		$Al_{0.71}Ga_{0.29}N$	GaN	$Al_{0.4}Ga_{0.6}N$	GaN	$Al_{0.4}Ga_{0.6}N$
Thickness	700 nm	690 nm		5 ML	6 ML	30 nm	4 ML	200 nm
N_d ($\times 10^{18}$ cm^{-3})	10	10	40	…	5	5 (1 nm)	5	10
Composition	AlN	$Al_{0.35}Ga_{0.65}N$		$Al_{0.63}Ga_{0.37}N$	GaN	$Al_{0.36}Ga_{0.64}N$	GaN	$Al_{0.35}Ga_{0.65}N$
Thickness	1000 nm	520 nm		5 ML	6 ML	10 nm	3 ML	40 nm
N_d ($\times 10^{18}$ cm^{-3})	10	10	20	…	10	…	10	10

electrons across the $Al_{.71}Ga_{.29}N$ injection barrier, which constitutes the electrical contact to our MQW at zero bias.

From the point of view of the strain management, the MQW is designed to be lattice matched to a commercial 700-nm-thick fully relaxed $Al_{0.4}Ga_{0.6}N$-on-sapphire template, grown by metalorganic vapor phase epitaxy (MOVPE). Only two layers are expected to be strained, namely, the 6-ML-thick GaN absorbing wells and the 5-ML-thick $Al_{.71}Ga_{.29}N$ injection barriers. Their relative lattice mismatch to the $Al_{0.4}Ga_{0.6}N$ template is −0.97% (compressive strain) and +0.76% (tensile strain), respectively. The opposite sign of the strain in those layers mutually compensate each other against lattice relaxation.[14,34]

The above-described structure will be referred hereafter as QWIP-on-AlGaN. A second design was performed following the same principles of device operation, but trying to keep the structure under compressive strain to prevent crack propagation associated with the thermal mismatch. It is known that the growth on an AlN buffer layer prevents both thermal- and mismatch-related cracking, but at the price of an increase in the threading dislocation density.[35] In this second design, the active MQW consists now of 20 periods of a 3-layer heterostructure containing a 6-ML-thick GaN well, a 10-nm-thick $Al_{0.36}Ga_{0.64}N$ escape barrier, and a 5-ML-thick $Al_{0.63}Ga_{0.37}N$ injection barrier. The top cap layer was 50-nm-thick n^+-$Al_{.35}Ga_{.65}N$ ($N_d = 1 \times 10^{19}$ cm^{-3}), the injection well was 3-ML-thick n^+-GaN ($N_d = 1 \times 10^{19}$ cm^{-3}), and the bottom contacting layer was 520 nm of n^+-$Al_{0.35}Ga_{0.65}N$ ($N_d = 1 \times 10^{19}$ cm^{-3}). The composition of 35% of Al in the AlGaN buffer layer was selected to match the average composition of the MQW. However, the lattice match is not guaranteed if the buffer layer is not fully relaxed. This uncertainty was the reason to keep the number of periods and the thickness of the $Al_{0.36}Ga_{0.64}N$ "escape barrier" to lower values than in the case of the QWIP-on-AlGaN. This second design will be referred hereafter as QWIP-on-AlN. Table I summarizes and compares both designs.

III. IMPLEMENTATION

Following the design from Fig. 2(a), the QWIP-on-AlGaN structure was grown by plasma-assisted molecular beam epitaxy (PAMBE) on a 700-nm-thick n^+-$Al_{0.4}Ga_{0.6}N$-on-sapphire template, doped with Si at $N_d = 10^{19}$ cm^{-3}. The growth was performed at a substrate temperature of 720 °C (calibrated by measurement of the Ga desorption[32]), under Ga rich conditions and without growth interruptions.[35] To do so, two Al cells were used, tuning their temperature to obtain Al mole fractions of 40% and 71%, and one Ga cell assured a continuous Ga excess during the growth. The growth rate was fixed by the flux of active nitrogen, which was 0.5 ML/s (≈450 nm/h).

Characterization by high-resolution x-ray diffraction (HRXRD) confirmed the nominal layer thickness. Figure 3(a) shows an ω–2θ diffractogram around the (0002) $Al_{0.4}Ga_{0.6}N$ reflection, together with a simulation using the GlobalFit software from Rigaku and assuming that the structure is fully strained on $Al_{0.4}Ga_{0.6}N$. The (0002) reflections associated with (i) the 700-nm-thick $Al_{0.4}Ga_{0.6}N$ template, (ii) the 690-nm-thick $Al_{0.4}Ga_{0.6}N$ buffer layer grown by PAMBE, (iii) the 1350-nm-thick MQW, and (iv) the 200-nm-thick $Al_{0.4}Ga_{0.6}N$ cap layer are merged into the peak located at $2\theta = 35.15°$. Note that the (0002) reflection of the $Al_{0.4}Ga_{0.6}N$-on-sapphire template was measured at $2\theta = 35.153°$ before the growth of the QWIP structure. Looking at the angular location of the satellites associated with the MQW reflection, this means that the difference in lattice parameter c between the MQW and the $Al_{0.4}Ga_{0.6}N$-on-sapphire template is <0.04%, which implies that the difference in Al composition is <1%.

High-resolution transmission electron microscopy (HRTEM) and high-angle annular dark field (HAADF) scanning transmission electron microscopy (STEM) images in the inset of Fig. 3(a) and in Fig. 3(b) confirm the nominal layer thicknesses and show sharp interfaces between the layers of the MQW. In optical and scanning electron microscope images, we detected the presence of some cracks in the epitaxial structure, separated by a typical distance of 30–50 μm, which originates at the $Al_{0.4}Ga_{0.6}N$/sapphire interface of the template. Such cracks were not observed in the $Al_{0.4}Ga_{0.6}N$ template prior to the PAMBE growth and might originate from the thermal mismatch of the AlGaN layers with the sapphire substrate.

We also grew a second QWIP structure following the QWIP-on-AlN design, using the same growth conditions as for the QWIP-on-AlGaN, but using a 1-μm-thick AlN-on-sapphire commercial MOVPE template as substrate. The structure was characterized by HRXRD with the results presented in Fig. 3(c). From the comparison of the experimental data with simulations, the AlGaN buffer layer is only partially relaxed, presenting a residual strain along the growth axis $\varepsilon_{zz} = (5.2 \pm 0.4) \times 10^{-3}$. This is consistent with the very slow relaxation process observed in III-nitride layers grown under metal-rich conditions by PAMBE.[35] On top of the buffer, the MQW evolves rapidly to a situation where its in-plane lattice parameter corresponds to that of a relaxed AlGaN layer which matches the average Al composition of the MQW.[36]

Both the QWIP-on-AlGaN and the QWIP-on-AlN devices were fabricated in the same processing run. The active mesa of 700×700 μm^2 was defined by optical photolithography and etched

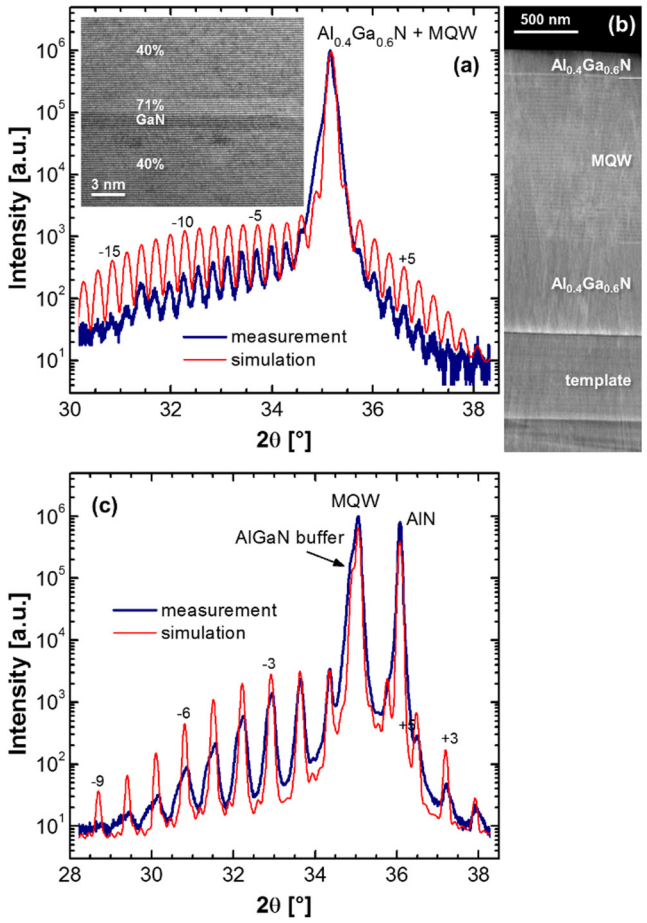

FIG. 3. (a) HRXRD ω–2θ scan of the (0002) reflection of the QWIP-on-AlGaN structure, together with a simulation that assumes that the structure is fully strained on the $Al_{0.40}Ga_{0.60}N$ template. Inset: HRTEM view of an $Al_{0.4}Ga_{0.6}N$/GaN/$Al_{0.71}Ga_{0.29}N$/$Al_{0.4}Ga_{0.6}N$ section in the middle of the MQW. (b) Low-resolution HAADF-STEM image of the entire QWIP-on-AlGaN. (c) HRXRD ω–2θ scan of the (0002) reflection of the QWIP-on-AlN structure, together with a simulation that assumes the MQW structure to be pseudomorphically grown with an in-plane lattice parameter that would correspond to that of a relaxed AlGaN layer with the average Al composition of the MQW. On the contrary, the AlGaN buffer layer is only partially relaxed.

down to the n+-bottom buffer layer by inductive coupled plasma (ICP) in Cl_2. The Ti/Al (30 nm/ 200 nm) bimetallic layer of the electrical contact was deposited by e-beam evaporation and annealed for 100 s in an H_2-N_2 atmosphere with 10 vol% H_2 at 425 °C, in a rapid thermal-annealing (RTA) reactor. The center of the top surface of the mesas was kept unmetallized to allow front illumination.

IV. DEVICE CHARACTERIZATION

The photodetectors were characterized electrically by measuring the dark current as a function of the applied bias. Measurements

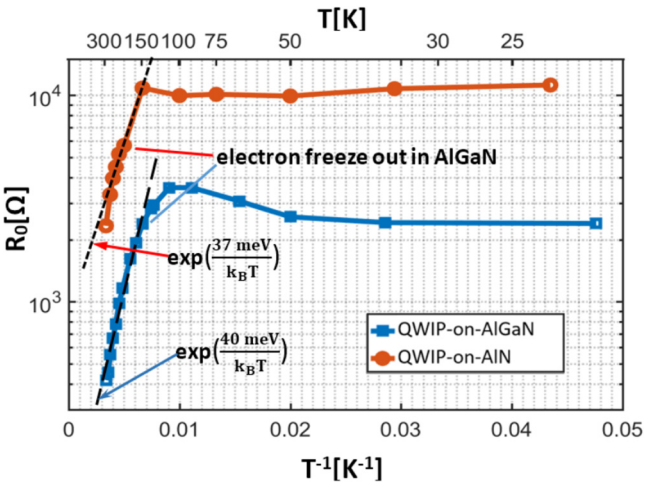

FIG. 4. Temperature dependence of the differential resistance at zero bias (R_0) for the QWIP-on-AlGaN and QWIP-on-AlN devices. A nearly exponential increase of R_0 with lowering the temperature is observed from 300 K down to 110 K (for the QWIP-on-AlGaN) and down to 150 K (for the QWIP-on-AlN). The black, dashed lines represent the exponential fit of the experimental data points to the dependence $R_0 = \exp(E_a/k_BT)$, where E_a activation energy and k_B-is the Boltzmann constant. The obtained values of activation energies were $E_a = 37$ and 40 meV for QWIP-on-AlN and QWIP-on-AlGaN, respectively, while k_B-is the Boltzmann constant.

were performed in the temperature range of 18–300 K, in order to study the internal dynamics of the devices. The differential resistance at zero bias (R_0) was calculated by applying a linear fit to the current-voltage relation around zero bias. The value of R_0 is inversely proportional to the dark current at $V \approx 0$ and is responsible for device thermal noise at zero bias. Figure 4 shows the temperature dependence of R_0 for the two devices under study. The value of R_0 is significantly lower for the QWIP-on-AlGaN compared to the QWIP-on-AlN. This is hard to understand based on the one-dimensional electrical transport model, since, in comparison with the QWIP-on-AlN design, the QWIP-on-AlGaN has an escape barrier that is three times thicker, twice the number of periods in the MQW, and a larger barrier height for electron escape from the GaN well. In addition, despite of the lower R_0, the QWIP-on-AlGaN had higher signal-to-noise (SNR) level in photocurrent measurements compared to the QWIP-on-AlN. The lower R_0 in the QWIP-on-AlGaN can be explained by parallel conduction through the vertical cracks. Note that such cracks were not observed in the QWIP-on-AlN structure, thus the vertical current flow should be more uniform in this latter case.

The plot of the temperature dependence of R_0 in Fig. 4 shows, for both devices, a nearly exponential increase of R_0 with lowering the temperature from 300 K down to 110 K (for the QWIP-on-AlGaN) and 150 K (for the QWIP-on-AlN). This is likely related to the freeze out of carriers in the AlGaN-escape barriers, which were nonintentionally doped (except for the modulation doping within a 1-nm-thick interval in the case of QWIP-on-AlGaN). The estimated activation energy for the observed process would be around 35–40 meV, which

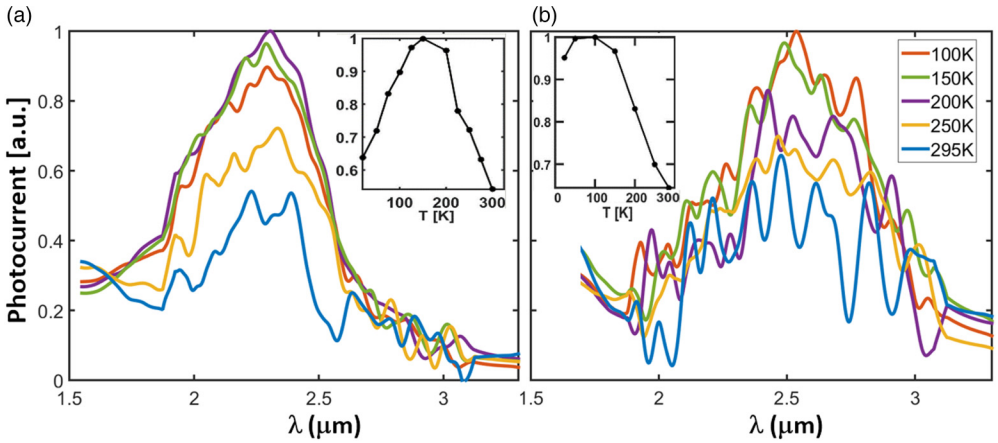

FIG. 5. Experimental photocurrent spectra of the (a) QWIP-on-AlGaN and (b) QWIP-on-AlN devices at various temperatures. Insets: Variation of the peak photocurrent (in arbitrary units) as a function of temperature.

is consistent with reported Si-donor ionization energy in $Al_{0.3}Ga_{0.7}N$ for low doping concentration ($<1\times10^{18}$ cm^{-3}).[33]

For photocurrent measurements, we used a Fourier transform infrared (FTIR) spectrometer equipped with an IR tungsten filament radiation source. The device was mounted on a copper plate attached to the cold finger of a cryostat in high vacuum. The sample was located at the focal point of the FTIR system. In front of the cryostat window, the incident beam was modulated by an optical chopper. The detector signal was amplified by a low noise transimpedance amplifier, whose output was read by a lock-in amplifier. The analog output of the lock-in amplifier was fed back to the FTIR system, which was operated in the step-scan mode. Temperature-dependent measurements were performed in the range from 300 to 14 K, in order to identify the physical processes limiting the response at room temperature and provide a view of the improvement potential of the devices.

The ISBT in the QWIP-on-AlGaN was set by the design to $\lambda = 2.3\,\mu$m, specifically near the center of one of the transmission atmospheric windows (between 2.0 and 2.5 μm) in the SWIR range. The experimental photocurrent peak wavelength in Fig. 5(a) shows a good match with the simulations, with the photocurrent peak precisely at 2.3 μm. The variation of the peak response as a function of temperature is presented as an inset in the figure. The highest response was observed at 150–200 K, and it was approximately twice as large as response at room temperature. The decrease in the responsivity in the 200 K to 300 K range might be associated with the expected decrease of the carrier mobility in the AlGaN-escape barriers, due to electron-phonon scattering.[37,38] The decrease of the photocurrent response at temperatures below 100 K can be again explained by the temperature dependence of the electron mobility in AlGaN, which at low temperatures is determined by scattering of electrons on ionized impurities, dislocations, and alloy inhomogeneities.[37,38]

In the case of the QWIP-on-AlN, the photocurrent spectra in Fig. 5(b) peak around $2.50\pm0.05\,\mu$m, which is in good agreement with the 2.54 μm predicted by the simulations. The measurement reflects systematically lower signal-to-noise ratio (SNR) compared to the QWIP-on-AlGaN, as shown in Fig. 5(a). In both cases, the SNR improves at lower temperatures. The response reaches its maximum value around 100 K (see the inset in the figure).

For the two devices, the relative spectral width of the photocurrent peaks, at all temperatures, was $d\lambda/\lambda \approx 30\%$. The lack of temperature dependence of the spectral width indicates that the broadening is due to an inhomogeneous mechanism, such as thickness fluctuations or alloy inhomogeneities.

The responsivity measurements were performed using free-space optical setup at room temperature, using a black body radiation source at 1000 K. The beam was modulated by an optical chopper and directed toward the front surface of the sample under 45° incidence angle. The resulting photocurrent was measured by a lock-amplifier.

Figure 6 shows the absolute responsivity at room temperature for the QWIP-on-AlGaN. A responsivity of 88 μA/W was measured at zero bias, increasing up to 302 μA/W at −1.0 V bias. Using the factor of 2 between the photocurrent at room temperature and

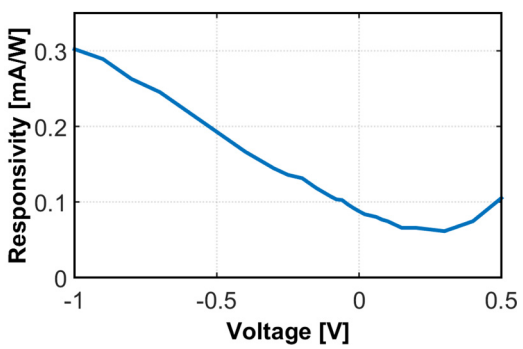

FIG. 6. Room-temperature responsivity vs bias voltage of the QWIP-on-AlGaN.

at 150–200 K, the estimated responsivity at peak temperature would be 176 μA/W at zero bias. The responsivity is asymmetric to positive and negative bias due to the asymmetric nature of the band structure of the device. Negative bias increases the internal electric field and enhances the drift of the excited electrons, while small positive bias reduces the internal electric field up to a point where the photocurrent reaches its minima. At that point, around 250 mV, the internal electric field in the escape barrier is nearly zero. A further increase of bias causes a band bending and drift to the opposite direction, motivating the increase in responsivity around 500 mV bias.

In the case of the QWIP-on-AlN, the recorded zero-bias responsivity was 40 μA/W at room temperature, which implies a peak responsivity of 62 μA/W at 100 K. Unfortunately, the application of bias to the QWIP-on-AlN caused a raise of the noise to the level, which prevented any further responsivity measurement.

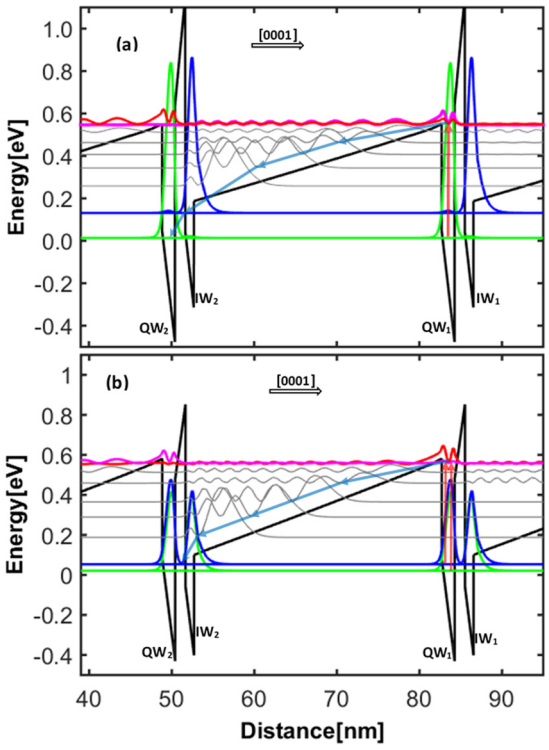

FIG. 7. Conduction band diagram (black, thick line) and squared wavefunctions of proposed two polar PV-QWIP GaN/AlGaN MQWs structures grown on an $Al_{0.37}Ga_{0.63}N$ template on the [1000] sapphire plane. The black block arrow indicates the growth direction. Selected wavefunctions from the "quasicontinuous" spectrum, which are localized in the $Al_{0.37}Ga_{0.63}N$ barrier, are drawn as grey lines, while those associated with the GaN quantum wells are drawn using green, blue, red, and magenta lines. The red vertical arrows illustrate the photoabsorption transition between electronic bound-to-quasibound state in the active QW in both designs. However, here, in order to increase the electric field in the escape barrier above 100 kV/cm, we propose to insert GaN injection well (IW) between injection and escape barriers. The diagonal blue arrows indicate "cascade" of possible paths of ISB scattering along the escape barrier toward the next ground absorption well via LO-phonon emission of energy, around 100 meV or higher. However, most intersubband transitions in the escape barrier can take place via lower energy transfer mediated, primarily, by acoustic phonon emission. (a) The first design uses thin injection well (IW) with a single localized state at energy around 100 meV above the ground state energy of the adjacent absorbing well. This design feature facilitates the fast electron transition from the state localized in injection well toward the ground state of the active well, mediated by LO-phonon emission. (b) The second design relies on strong coupling between ground states of adjacent active and injection GaN wells. Consequently, the blocking electrons from injection to GaN absorbing well by $Al_{0.60}Ga_{0.40}N$ injection barrier is virtually removed, thanks to the resonant tunneling between ground states of both GaN wells.

V. FUTURE GaN/AlGaN QWIP DETECTOR

In order to improve the responsivity of our PV-QWIPs, we need a higher electric field in the AlGaN "escape barrier" layer at zero voltage bias. The increase of the internal field to the level above 100 kV/cm can be achieved by adding a GaN "injection well" between the "injection barrier" and the "escape barrier," as illustrated in Fig. 7(a). This QWIP architecture consists of a 6-ML-thick n^+-GaN-active well, a 30-nm-thick $Al_{0.37}Ga_{0.63}N$ escape barrier, a 4-ML-thick GaN injection well, and a 5-ML-thick $Al_{0.60}Ga_{0.40}$ N "injection barrier." The structure is assumed to be lattice matched to relaxed $Al_{0.37}Ga_{0.63}N$ template. In this design, transport along the escape barrier will likely combine LO-phonon inelastic scattering (cascading) and classical electron drift. Examples of LO-phonon "cascades" in the escape barrier are marked with blue arrows in Fig. 7(a), with the corresponding subband states that participate in the cascading process marked with red color.

The conduction band profile in Fig. 7(a) has apparent similarity to the QCD band diagram of Sakr *et al.*,[21] but the layer sequence is significantly different and the photocurrent should follow the opposite crystallographic direction. With respect to such QCD, our design presents an improved escape probability, since we rely on bound-to-quasibound ISBTs in the active wells, in contrast with the bound-to-bound ISBT in the QCD design.[21] More importantly, our design presents a major improvement in the coupling of the low-energy edge of the escape barrier with the ground state of the next active well.

As an alternative to assure the efficient current flow through the injection barrier, without compromising the high field in the escape barrier, we propose a further design improvement, in which "injection" and "absorbing wells" are strongly coupled [see Fig. 7(b)].

VI. SUMMARY AND CONCLUSION

We presented a method of design of bound-to-quasibound QWIPs based on polar GaN/AlGaN MQWs, using a long-period (13–33 nm) MQW structure. The period of the MQW consists of 3 layers, namely, the active quantum well, an escape barrier, and an injection barrier. This asymmetric-barrier MQW structure allows a partial compensation of the polarization-related internal electric field in the escape barrier, which approaches the band profile to that implemented in polarization-free III-V compound semiconductors. With this principle, a photovoltaic QWIP was demonstrated operating at 2.3 μm peak wavelength, with a room-temperature responsivity of 88 μA/W at 45° front illumination angle. The responsivity increased roughly linearly with an applied negative bias to the top contact, at the approximate rate of 210 μA/W/V. It was established,

within the error of high-resolution x-ray diffraction measurement, that the entire detector epistructure, which included a 40-period MQW with 30-nm-thick barriers and the contact layers, of combined thickness over 900 nm, was grown pseudomorphically on an AlGaN-on-sapphire template. The possible difference in Al composition between the template and the MQW was <1%.

Finally, we propose two new designs for future implementation, which should result in a performance enhancement due to the increase of the electric field in the extraction barrier and improved coupling of the low-energy edge of the escape barrier with the ground level of the active well. These improvements rely on the introduction of a fourth layer in the period, a GaN injection well, which can be strongly coupled to the active well to facilitate the electron transfer to the next period. In this configuration, the electron transport in the escape barrier combines classical electron drift with LO-phonon inelastic scattering in a cascade process.

ACKNOWLEDGMENTS

We are grateful to Dr. Kwang K. Choi for valuable discussion, and Svetlana Yofis and Yossi Leybovitz for help in device fabrication. We acknowledge financial support under Technion-MOD Contract Nos. 2024773 and 2024154.

REFERENCES

[1]S. W. Sanderson and K. L. Simons, Res. Policy **43**, 1730 (2014).
[2]I. F. Akyildiz, J. M. Jornet, and C. Han, Phys. Comm. **12**, 16 (2014).
[3]K. Ahi, Opt. Eng. **56**, 090901 (2017).
[4]J. D. Brown, R. Borges, E. Piner, A. Vescan, S. Singhal, and R. Therrien, Solid State Electron. **46**, 1535 (2002).
[5]T. Boles, AIP Conf. Proc. **1934**, 020001 (2018).
[6]R. McClintock and M. Razeghi, Proc. SPIE, **9555**, 955502 (2015).
[7]N. Iizuka, K. Kaneko, N. Suzuki, T. Asano, and S. Noda, O Wada, Appl. Phys. Lett. **77**, 31 (2000).
[8]B. F. Levine, J. Appl. Phys. **74**, 15 (1993).
[9]A. Rogalski, Int. J. High Speed Electron Syst., **12**, 593 (2002).
[10]D. Gunapala, S. V. Bandara, J. K. Liu, J. M. Mumolo, D. Z. Ting, C. J. Hill, J. Nguyen, and S. B. Rafol, Proc. SPIE, **7660**, 76603L (2010).
[11]H. Schneider, S. Ehret, E. C. Larkins, and J. D. Ralston, in *Quantum Well Intersubband Transition Physics and Devices*, edited by H. C. Liu, B. F. Levine, and J. Y. Andersson (Kluwer Academic Publishers, 1994), pp. 187–196.
[12]C. Schonbein, H. Schneider, G. Bihlmann, K. Schwarz, and P. Koidl, App. Phys. Lett. **68**, 973 (1996).
[13]E. Luna, J. L. Sánchez-Rojas, A. Guzmán, J. M. G. Tijero, and E. Muñoz, IEEE Photon. Tech. Lett, **15**, 105 (2003)
[14]K. T. Lai, S. K. Haywood, A. H. Mohamed, M. Missous, and R. Gupta, Appl. Phys. Lett. **87**, 192113 (2005).
[15]D. Hofstetter, S. -S. Schad, H. Wu, W. J. Schaff, and L. Eastman, Appl. Phys. Lett. **83**, 572 (2003).
[16]D. Hofstetter, E. Baumann, F. R. Giorgetta, M. Graf, M. Maier, F. Guillot, E. Bellet-Amalric, and E. Monroy, Appl. Phys. Lett. **88**, 121112 (2006). D. Hofstetter, E. Baumann, F. R. Giorgetta, F. Guillot, S. Leconte, and E. Monroy, Appl. Phys. Lett. **91**, 131115 (2007); D. Hofstetter, E. Baumann, F. R. Giorgetta, J. Dawlaty, P. A. George, F. Rana, F. Guillot, and E. Monroy, Appl. Phys. Lett. **92**, 231104 (2008).
[17]F. F. Sudradjat, W. Zhang, J. Woodward, H. Durmaz, T. D. Moustakas, and R. Paiella, Appl. Phys. Lett. **100**, 241113 (2012).
[18]L. Gendron, M. Carras, A. Huynh, V. Ortiz, C. Koeniguer, and V. Berger, Appl. Phys. Lett. **85**, 2824 (2004).
[19]A. Vardi, G. Bahir, F. Guillot, C. Bougerol, E. Monroy, S. E. Schacham, M. Tchernycheva, and F. H. Julien, Appl. Phys. Lett. **92**, 011112 (2008); A. Vardi, N. Kheirodin, L. Nevou, H. Machhadani, L. Vivien, P. Crozat, M. Tchernycheva, R. Colombelli, F. H. Julien, F. Guillot, C. Bougerol, E. Monroy, S. Schacham, and G. Bahir, Appl. Phys. Lett. **93**, 193509 (2008).
[20]A. Vardi, S. Sakr, J. Mangeney, P. K. Kandaswamy, E. Monroy, M. Tchernycheva, S. E. Schacham, F. H. Julien, and G. Bahir, Appl. Phys. Lett. **99**, 202111 (2011).
[21]S. Sakr, E. Giraud, M. Tchernycheva, N. Isac, P. Quach, E. Warde, N. Grandjean, and F. H. Julien, Appl. Phys. Lett. **101**, 251101 (2012); A. Pesach, S. Sakr, E. Giraud, O. Sorias, L. Gal, M. Tchernycheva, M. Orenstein, N. Grandjean, F. H. Julien, and G. Bahir, Opt. Express **22**, 21069 (2014).
[22]M. Beeler, E. Trichas, and E. Monroy, Semicond. Sci. Technol. **28**, 074022 (2013).
[23]H. Machhadani, M. Beeler, S. Sakr, E. Warde, Y. Kotsar, M. Tchernycheva, M. P. Chauvat, P. Ruterana, G. Nataf, P. De Mierry, E. Monroy, and F. H. Julien, J. Appl. Phys. **113**, 143109 (2013).
[24]H. Durmaz, D. Nothern, G. Brummer, T. D. Moustakas, and R. Paiella, Appl. Phys. Lett. **108**, 201102 (2016).
[25]A. Pesach, E. Gross, C.-Y. Huang, Y.-D. Lin, A. Vardi, S. E. Schacham, S. Nakamura, and G. Bahir, Appl. Phys. Lett. **103**, 022110 (2013).
[26]C. Edmunds, J. Shao, M. Shirazi-HD, M. J. Manfra, and O. Malis, Appl. Phys. Lett. **105**, 021109 (2014).
[27]T. Kotani, M. Arita, and Y. Arakawa, Appl. Phys. Lett. **105**, 261108 (2014).
[28]C. B. Lim, A. Ajay, C. Bougerol, B. Haas, J. Schoermann, M. Beeler, J. Laehnemann, M. Eickhoff, and E. Monroy, Nanotechnology **26**, 435201 (2015).
[29]B. Lim, M. Beeler, A. Ajay, J. Laehnemann, E. Bellet-Amalric, C. Bougerol, and E. Monroy, J. Appl. Phys. **118**, 014309 (2015).
[30]S. V. Bandara, S. D. Gunapala, D. Z.-Y. Ting, S. B. Rafol, and J. K. Liu, in GaAs/AlGaAs Sub-mm & MM Detector Technology Workshop, Monterey, CA, 1–3 April 2002; S. V. Bandara and S. D. Gunapala, *Intersubband Transitions in Quantum Wells. Physics and Device Applications I*, Semiconductors and Semimetals, 197 ed., edited by H. C. Liu and F. Capasso (Academic Press, 2000), Vol. 62.
[31]S. Birner, T. Zibold, T. Andlauer, T. Kubis, M. Sabathil, A. Trellakis, and P. Vogl, IEEE Trans. Electron Devices **54**, 2137 (2007).
[32]P. K. Kandaswamy, F. Guillot, E. Bellet-Amalric, E. Monroy, L. Nevou, M. Tchernycheva, A. Michon, F. H. Julien, E. Baumann, F. R. Giorgetta, D. Hofstetter, T. Remmele, M. Albrecht, S. Birner, and L. S. Dang, J. Appl. Phys. **104**, 093501 (2008).
[33]K. Zhu, M. L. Nakarmi, K. H. Kim, J. Y. Lin, and H. X. Jiang, Appl. Phys. Lett., **85**, 4669 (2015).
[34]S. A. Al Muyeed, W. Sun, X. Wei, R. Song, D. D. Koleske, N. Tansu, and J. J. Wierer, AIP Adv. **7**, 105312 (2017).
[35]E. Bellet-Amalric, C. Adelmann, E. Sarigiannidou, J. L. Rouviere, G. Feuillet, E. Monroy, and B. Daudin, J. Appl. Phys. **95**, 1127 (2004).
[36]Y. Kotsar, B. Doisneau, E. Bellet-Amalric, A. Das, E. Sarigiannidou, and E. Monroy, J. App. Phys. **110**, 033501 (2011).
[37]M. Ahoujja, Y. K. Yeo, and R. L. Hengehold, J. E. Van Nostrand, Appl. Phys. Lett. **80**, 25 (2002).
[38]M. Ahoujja, J. L. McFall, Y. K. Yeo, R. L. Hengehold, and J. E. Van Nostrand, Mat. Sci. Eng. **285**, B91–B92 (2002).